



Published in final edited form as:

Curr Biol. 2020 April 06; 30(7): 1269–1274.e2. doi:10.1016/j.cub.2020.01.040.

A Color Vision Circuit for Non-Image-Forming Vision in the Primate Retina

Sara S. Patterson^{1,2}, James A. Kuchenbecker², James R. Anderson³, Maureen Neitz², Jay Neitz^{2,4,*}

¹Graduate Program in Neuroscience, University of Washington, Seattle, WA, 98195, USA

²Department of Ophthalmology, University of Washington, Seattle WA, 98195, USA

³Department of Ophthalmology and Visual Sciences, John A. Moran Eye Center, University of Utah School of Medicine, Salt Lake City, UT, 84132, USA

⁴Lead Contact

SUMMARY

Melanopsin-expressing, intrinsically photosensitive retinal ganglion cells (ipRGCs) synchronize our biological clocks with the external light/dark cycle [1]. In addition to photoentrainment, they mediate the effects of light experience as a central modulator of mood, learning and health [2]. This makes a complete account of the circuitry responsible for ipRGCs' light responses essential to understanding their diverse roles in our wellbeing. Considerable progress has been made in understanding ipRGCs' melanopsin-mediated responses in rodents [3–5]. However, in primates, ipRGCs also have a rare blue-OFF response mediated by an unknown short wavelength sensitive (S) cone circuit [6]. Identifying this S-cone circuit is particularly important as ipRGCs mediate many of the wide-ranging effects of short-wavelength light on human biology. These effects are often attributed to melanopsin, but there is evidence for an S-cone contribution as well [7,8]. Here, we tested the hypothesis that the S-OFF response is mediated by the S-ON pathway through inhibitory input from an undiscovered S-cone amacrine cell. Using serial electron microscopy in the macaque retina, we reconstructed the neurons and synapses of the blue cone connectome, revealing a novel inhibitory interneuron, an amacrine cell, receiving excitatory glutamatergic input exclusively from S-ON bipolar cells. This S-cone amacrine cell makes highly selective inhibitory synapses onto ipRGCs, resulting in a blue-OFF response. Identification of the S-cone amacrine cell provides the missing component of an evolutionarily-ancient circuit using spectral information for non-image forming visual functions.

*Correspondence: jneitz@uw.edu.

AUTHOR CONTRIBUTIONS

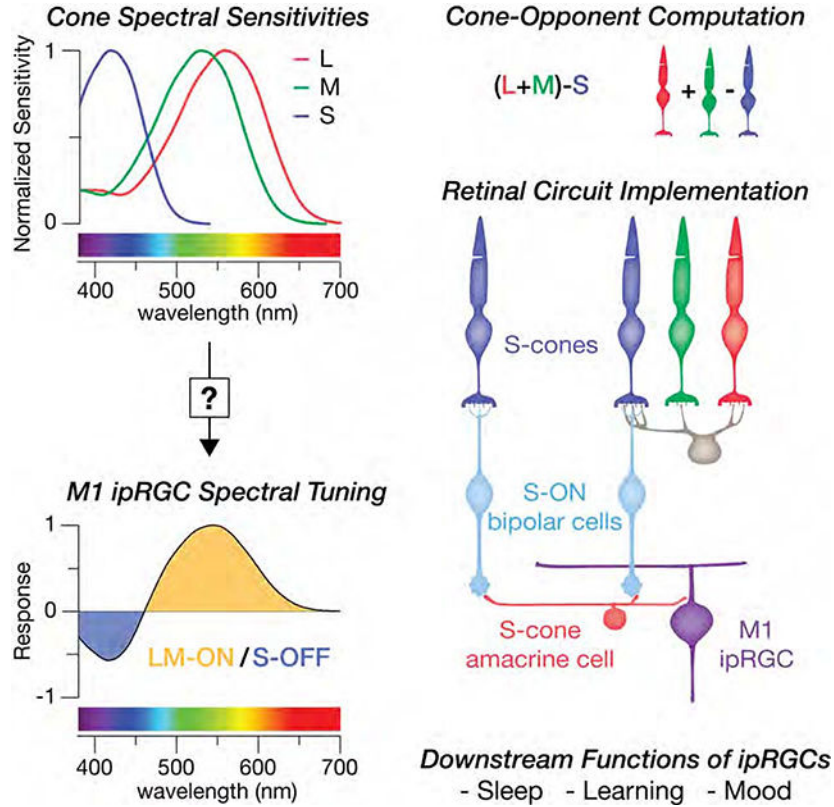
J.N., M.N. and S.P. conceived the project, designed experiments and wrote the paper. J.K., J.N. and M.N. acquired the volume. J.A. and J.K. built the volume. J.A. created the annotation software. S.P. created the visualization software, performed the experiments and analyzed the data.

DECLARATION OF INTERESTS

The University of Washington has submitted provisional patent application (628504893) disclosing Systems, Methods and Devices for Stimulating Circadian Rhythms (Authors: S.P., J.K., M.N., J.N.).

Publisher's Disclaimer: This is a PDF file of an unedited manuscript that has been accepted for publication. As a service to our customers we are providing this early version of the manuscript. The manuscript will undergo copyediting, typesetting, and review of the resulting proof before it is published in its final form. Please note that during the production process errors may be discovered which could affect the content, and all legal disclaimers that apply to the journal pertain.

Graphical Abstract



RESULTS

3D Reconstruction of the Primate S-Cone Connectome

Primate ipRGCs have a rare yellow-ON, blue-OFF color tuning and respond to increased activity in L- and M-cone pathways and decreased activity in S-cone pathways (i.e. LM-ON/S-OFF cone opponency) [6]. The neural basis for the ipRGC’s color tuning remains an open question. The S-OFF responses are blocked by L-AP4, an ON pathway agonist, indicating an amacrine cell inhibition may invert the output of S-ON bipolar cells [9–12]. However, the mammalian retina contains 20–40 amacrine cell types, making selective identification of one undiscovered type difficult [13,14]. Moreover, due to the rarity of S-cones [15], little is known about the diversity of pathways carrying S-cone signals. To investigate the circuit mechanisms responsible for the ipRGC’s S-OFF response, we used serial electron microscopy (EM) to reconstruct the neurons and synapses of the primate S-cone connectome from a volume of macaque inferior retina at ~1–1.5 mm eccentricity, near the peak density for ipRGCs [16]. The resulting dataset of nearly 2000 sections spanned from the outer nuclear layer to the nerve fiber layer, enabling us to reconstruct complete circuits in 3D and identify the synaptic contacts between neurons.

Reliable identification of upstream S-cone circuitry is essential for identifying a novel S-cone neuron, thus, we began by reconstructing the established S-cone connectome, building

on our previous reconstructions of S-cone bipolar cells in the outer retina [17]. Briefly, S-cones were distinguished from L/M-cones by their highly stereotyped post-synaptic contacts [18]. Each S-cone provides input to one to three S-ON bipolar cells and a single OFF midget bipolar cell (Figure 1A). The S-ON bipolar cells are highly cone-type specific and contact multiple S-cones, often passing multiple L/M-cones without contact to reach neighboring S-cones [19]. Using these features, we confidently identified eight S-cones and 14 S-ON bipolar cells.

Here, we extended these S-ON pathway reconstructions to the inner retina. The terminals of each bipolar cell type stratify at a stereotyped location within the inner retina, providing excitatory glutamatergic input to co-stratifying amacrine and retinal ganglion cells (RGCs) within the same layer [20]. Each of the 14 S-ON bipolar cells stratified in the innermost layer of the inner retina, sublamina 5 (S5), closest to the ganglion cell layer (GCL) [19] (Figure 1A, 1B). We further verified S-ON bipolar cell identity by reconstructing their best known output: small bistratified RGCs (Figure 1B, 1C) [21,22]. Each S-ON bipolar cell contacted two or three small bistratified RGCs and the most complete small bistratified RGCs collected inputs from up to nine S-ON bipolar cell terminals. The S-cone exclusive inner dendritic tier of each small bistratified RGC served as a bridge within the inner retina to identify an additional 46 S-ON bipolar cell terminals. In total, we reconstructed 60 S-ON bipolar cell terminals, each confirmed by extensive synaptic contacts with least one of 12 small bistratified RGCs (Figure 1D).

A novel S-cone selective amacrine cell links S-ON bipolar cells to ipRGCs

We next reconstructed the two major ipRGC subtypes reported in the primate retina, which are distinguished by their stratification in the outermost and innermost edges of the inner retina and are thought to correspond to M1 and M2 ipRGCs, respectively [16,23,24] (Figure 1E). The dendrites of both ipRGCs branched sparsely, with dendritic fields extending beyond the edges of the volume. We focused our efforts on M1 ipRGCs with somas in the GCL and dendrites stratifying primarily in the outermost layer of the inner retina, sublamina 1 (S1). As shown in Figure 3J, this morphology limits the opportunities for contact with amacrine cells receiving S-ON bipolar cell input in S5.

Taken together, our reconstructions of the established S-cone circuitry and ipRGCs provided the necessary infrastructure to effectively search for the source of the S-OFF response. To identify candidate S-cone amacrine cells, we reconstructed neurons post-synaptic to the ribbon synapses in S-ON bipolar cell terminals. While many amacrine cells stratifying in S5 received occasional S-ON bipolar cell input, a population of medium-field displaced amacrine cells recognizable by their distinctive soma ultrastructure (Figure 2D) were ultimately identified as exclusively contacting S-ON bipolar cells (Figure 2C). In the inner retina, the amacrine cells' thin, sparse processes co-stratified narrowly with the S-ON bipolar cell terminals in S5. Their dendritic fields covered the S-ON bipolar cell terminal mosaic, each collecting input from over ten S-ON bipolar cell terminals. Of the 102 bipolar cell inputs to the three most complete amacrine cells, all but six were from confirmed S-ON bipolar cells.

Amacrine cell processes are typically confined to the inner retina, however, some S-cone amacrine cells also extended processes into the GCL. Strikingly, these processes contacted an M1 ipRGC soma (Figure 3A, Video S1). Moreover, thin branches extended from the ipRGC's cell body to receive additional input from the S-cone amacrine cell processes. Small branches extending from the primary dendrites were also observed receiving input from S-cone amacrine cells within the inner retina (Figure 3F, 3G).

M1 ipRGCs receive targeted synaptic input from S-cone amacrine cells

We next examined the synaptic connections between S-cone amacrine cells and ipRGCs, focusing on the three most complete reconstructions. Conventional synapses, which are traditionally assumed to be inhibitory, were identified as a cluster of vesicles on the pre-synaptic neuron adjacent to a membrane density on the post-synaptic neuron. Figure 3B–3E and 3H show S-cone amacrine cell synapses onto the ipRGC soma and branches within the inner retina and GCL. This unique concentration of S-cone-exclusive inhibition near the action potential initiation site could provide modulatory control over synaptic inputs received throughout the ipRGC's dendritic field [25]. The somas of human ipRGCs and other RGCs have been reported to receive GABAergic input [24,26,27] and the S-cone amacrine cell's morphology is consistent with a GABAergic amacrine cell [28]. Moreover, this motif is distinct from the previously identified glycinergic S-cone amacrine cell in ground squirrel that stratifies diffusely, collecting S-ON bipolar cell input in S5 and providing S-cone inhibition to non-ipRGC ganglion cells stratifying in S1 [10,29]. Based on strong morphological similarities, stratification and displaced soma, the primate S-cone amacrine cell is likely the homolog to the MA-S5 amacrine cell in mouse [30] and the A12 amacrine cell in human, cat and ground squirrel [31].

To visualize the extent of S-cone convergence onto M1 ipRGCs, we plotted the network of upstream S-cone exclusive circuits (Figure 3I). Each S-ON bipolar cell collects input from an overlapping set of 2–3 S-cones, as in Figure 1A. The network in Figure 3I is likely an underestimate at both the level of S-ON bipolar input to S-cone amacrine cells and S-cone amacrine cell input to ipRGCs, as we only included ipRGCs with somas within our EM volume and occasional S-cone amacrine cell processes extended past the edges of the volume or could not be reliably annotated. Nevertheless, the high degree of S-cone convergence suggests S-cone amacrine cell input to M1 ipRGCs contributes a strong S-cone signal.

DISCUSSION

Short-wavelength cone exclusive ON bipolar cells are a highly conserved feature of mammalian retinas [32,33] forming the basis of the primordial color vision circuit comparing long and short-wavelength light [34]. Here, we show that this circuit extends to the inner retina, with an additional S-cone exclusive neuron, an amacrine cell receiving only S-ON bipolar cell input. The concept of a primordial color vision circuit has been considered as the precursor to the primate hue perception circuitry, however, our findings suggest this ancient color vision circuit is instead still serving its original function. Much of the S-cone amacrine cell's output is targeted to ipRGCs, another highly conserved neuron mediating

ancient non-image-forming visual functions. Accordingly, the S-cone amacrine cell may be part of an evolutionarily ancient color vision circuit, not for hue perception, but for non-image-forming vision.

The downstream functions of the M1 ipRGCs are among the best characterized of all RGCs [35]. Thus, our results establish the S-cone amacrine cell among the few amacrine cell types to be placed within the context of a specific retinal circuit with an established visual function. The high degree of cone specificity demonstrated in Figure 2C indicates a crucial role for the S-cone amacrine cell. For example, the evolutionary pressure to know the time of day is strong and color-opponent circadian photoentrainment is well-established in many vertebrates [36,37]. As the sun rises and sets, the spectral contrast of the sky changes dramatically, with peaks in L/M- vs. S-cone contrast at sunrise and sunset [38–40]. The S-cones providing input to the S-cone amacrine cell receive feedback from L/M-cones, effectively encoding the S-cone contrast relative to L/M-cone contrast [41]. This cone-opponent signal is conveyed to inner retinal neurons by the S-ON bipolar cells [42]. Thus, the output of the S-cone amacrine cell is predicted to be color-opponent (S-ON/LM-OFF) and is well-suited to encode the reliable circadian changes in the color of the sky.

STAR METHODS

Lead Contact and Materials Availability

Further information and requests for resources should be directed to and will be fulfilled by the Lead Contact, Jay Neitz (jneitz@uw.edu). This study did not generate any new unique reagents.

Experimental Model and Subject Details

Retinal tissue was obtained from a terminally anesthetized male macaque (*Macaca nemestrina*) monkey through the Tissue Distribution Program at the Washington National Primate Center. All procedures were approved by the Institutional Animal Care and Use Committee at the University of Washington.

METHOD DETAILS

Microscopy

The tissue was imaged using a Zeiss Sigma VP field emission scanning electron microscope equipped with a 3View system and sectioned in the horizontal plane. Tissue preparation and image collection were optimized in signal-to-noise ratio for visualizing small, low contrast features such as synaptic ribbons that have previously been a challenge for serial block-face scanning (Figure 2A, 2B). In each 90 nm section, an area approximately 200 μm on a side was imaged as a 5 X 5 montage at a resolution of 7.5 nm/pixel. The volume contained 1893 horizontal 90 nm sections from the ganglion cell layer through the cone pedicles. Image registration was performed using Normir (<http://normir.github.io>).

Tissue Preparation

A block of inferior parafoveal retinal tissue at 1 mm eccentricity from the fovea center was processed as previously described [44]. A transmission electron microscopic image of a cross-section of the retina can be seen in Figure 1A of our previously published work [17]. Briefly, the eyecup was placed in 4% glutaraldehyde in 0.1M sodium cacodylate buffer pH 7.4 and while in this solution a 1 mm square of retina centered 1.5 mm inferior to the center of the fovea was cut out and then fixed overnight at 4° C. The tissue was next washed 5 × 5 minutes in 0.1M cacodylate buffer, then post fixed in osmium ferrocyanide for 1 hour on ice. The tissue was next washed 5 × 5 minutes in double distilled (dd)H₂O at room temperature (RT) and incubated in a 1% thiocarbohydrazide solution for 20 minutes at RT. The tissue was washed 5 × 5 minutes in ddH₂O and placed in 2% osmium tetroxide for 30 minutes at RT. The tissue was next washed 5 × 5 minutes in ddH₂O and en block stained in 1% uranyl acetate, (aqueous), overnight in the refrigerator. The next day the tissue was washed 5 × 5 minutes in ddH₂O, then en bloc stained in Walton's lead aspartate for 30 minutes at 60° C. The tissue was next washed 5 × 5 minutes in ddH₂O and dehydrated in ice cold 30%, 50%, 70%, and 95% ETOH, then allowed to come to RT. This was followed by 2 changes of 100% ETOH and two changes of propylene oxide. The tissue was then infiltrated in a 1:1 mixture of propylene oxide:Durcupan resin, for 2 hours and then infiltrated overnight in fresh Durcupan. The next day the tissue was given a fresh change of Durcupan for two hours and then placed in flat embedding molds and polymerized in a 60 ° C oven for two days. The block was then trimmed to approximately 0.5 mm². At this eccentricity (the edge of the foveal slope), the displacement of RGCs from cone pedicles was minimized while still remaining in a region where most midget RGCs receive single cone input.

Annotation

The serial EM volumes were annotated using the web-based, multiuser Viking software described previously (<http://connectomes.utah.edu>) [45]. Neuronal processes were traced through the sections by placing a circular disc at the structure's center of mass and linking the disc to annotations on neighboring sections. Compared to contouring [46] and skeleton reconstruction [47], this connectomics approach provided an optimal balance of efficiency and resolution for circuit-level research questions [45,48]. There were two exceptions to the disc annotations. Cone pedicles were outlined using a closed curve polygon defined by three or more control points. The detailed morphological reconstruction in Figure 3G was obtained by manually tracing the outlines of each dendritic process.

Synapses were annotated with lines connected by 2–3 control points and linked to a parent neuron. Synapse identification used previously described parameters [49]. The boundaries of the inner plexiform layer were determined locally and marked throughout the volume with a total of 258 markers for the inner nuclear layer (INL) boundary and 453 markers for the IPL-ganglion cell layer (GCL) boundary.

Data Analysis and Visualization

Data analysis and 3D rendering were performed using SBFSEM-tools, an open-source Matlab (Mathworks) program developed in the Neitz lab (<https://github.com/neitzlab/sbfsem-tools>) [17,48]. Final figures were compiled in Adobe Illustrator.

The cone pedicle locations in Figure 1A were based on XYZ coordinates of the closed curve annotation control points, connected by Catmull-Rom splines. The detailed morphology reconstructions in Figure 3G was obtained by extracting the coordinates from a stack of manually annotated processes. These coordinates were used to build a volume from which isosurfaces were extracted with a marching cubes algorithm then rendered as a triangle mesh. All other analyses and visualizations were performed using the X, Y, Z coordinates and radius of each annotation. The 3D models are triangle meshes built by rendering segments of connected annotations as rotated cylinders centered at each annotations' XYZ coordinates and scaled by their radii.

INL-IPL and GCL-IPL boundary surfaces were fit to the X, Y and Z coordinates of each IPL boundary marker type using bicubic interpolation. IPL depth could then be calculated for each annotation individually. Given an annotation's X, Y coordinates, the surfaces supplied the depth of the IPL boundaries at that X,Y location. The annotation's Z coordinate relative to the Z coordinates of each boundary could be calculated to determine percent IPL depth.

Cell Type Identification

In addition to the S-ON bipolar cell verification described in the text and our previous work [17], we also verified the S-ON bipolar cells were distinct from the other two bipolar cell inputs stratifying in S5. The morphology of our DB6 reconstructions matched previous reports [43,50]. A reliable parameter for distinguishing S-ON and DB6 bipolar cells is the smaller diameter of their axon terminal branches. Rod bipolar cell terminals were distinguished by input exclusively from rod photoreceptors in the outer retina and an absence of ribbon synapses onto RGCs in the inner retina.

To verify the identity of outer-stratifying (M1) ipRGCs, our strongest criteria was the dendritic stratification depth at the IPL-INL border [23,24,51]. Of all reported primate RGCs, M1 ipRGCs stratify closest to the inner nuclear layer (giant sparse monostratified [52]). The next closest RGC to the inner nuclear layer is the large sparse monostratified RGC, which stratifies around 30% IPL depth [52,53]. The M1 ipRGCs in this study stratified between 0–20%. Some primary dendrites of the M1 ipRGCs with somas in the ganglion cell layer travelled through S5 for tens of microns before descending to S1. However, all primary dendrites either reached S1 or ran off the edge of the volume. Displaced M1 ipRGCs are the only known RGC with a soma in the INL, providing further confirmation for the displaced M1 ipRGC (green) in Figure 1E, which stratified closest to the INL, had a large soma with significant synaptic input from a single amacrine cell type and a single axon with an ultrastructure and morphology matching the axons of RGCs in the ganglion cell layer. We also confirmed the presence of previously reported synaptic inputs. M1 ipRGCs receive some ON bipolar cell input in S1 from *en passant* synapses from DB6 bipolar cell axons, as well as other non-DB6 bipolar cell input presumed to be from DB1 bipolar cells [43]. We observed both M1 ipRGCs receiving infrequent bipolar cell input in S1 from neurons matching the morphology of DB1 bipolar cells [54,55]. Several DB6 bipolar cell axons were reconstructed, however, *en passant* ribbon synapses in bipolar cell axons are smaller than ribbon synapses in bipolar cell terminals [56] and were difficult to reliably identify with our volume's resolution. No contacts were observed between ipRGC

dendrites and S-ON bipolar cells or the S-cone OFF midget bipolar cells identified in our previous work [17]. In one case, appositions between a rod bipolar cell and an M1 ipRGC dendrite were observed [24,57]. As previously reported, a single type of amacrine cell made large inhibitory synapses along the dendrites of M1 ipRGCs and the soma of the displaced M1 ipRGC. While none were traced back to a soma, their morphology was consistent with dopaminergic amacrine cells reported to provide extensive synaptic input to M1 ipRGC somas and dendrites [16].

Quantification and Statistical Analysis

No statistical tests were used in the manuscript.

Data and Code Availability

The 3D reconstructions from Viking Viewer annotations are visualized with SBFSEM-tools, an open-source MATLAB toolbox (<https://github.com/neitzlab/sbfsem-tools>). The Viking Viewer software for visualizing both the dataset and the annotations is freely available (<http://connectomes.utah.edu>). Raw data and additional analysis code will be provided upon request by the Lead Contact, Jay Neitz (jneitz@uw.edu).

Supplementary Material

Refer to Web version on PubMed Central for supplementary material.

ACKNOWLEDGEMENTS

We thank Fred Rieke for helpful discussions, Andrea Bordt, David Marshak and Judy Ogilvie sharing their serial EM expertise and Ed Parker for excellent technical assistance. Tissue was provided by the Tissue Distribution Program at the Washington National Primate Research Center (WaNPRC) with the help of Chris English. This work was supported by NIH grants R01-EY027859 (J.N.), T32-NS099578 (S.P.), T32-EY07031 (S.P.), R01-EY028927 (J.A.), P30-EY001730, P30-EY014800 and Research to Prevent Blindness.

REFERENCES

1. Berson DM (2003). Strange vision: Ganglion cells as circadian photoreceptors. *Trends Neurosci.* 26, 314–320. [PubMed: 12798601]
2. LeGates TA, Fernandez DC, and Hattar S (2014). Light as a central modulator of circadian rhythms, sleep and affect. *Nat. Rev. Neurosci.* 15, 443–454. [PubMed: 24917305]
3. Milner ES, and Do MTH (2017). A Population Representation of Absolute Light Intensity in the Mammalian Retina. *Cell* 171, 865–866.e16. [PubMed: 28965762]
4. Berson D, Dunn F, and Takao M (2002). Phototransduction by retinal ganglion cells that set the circadian clock. *Science.* 295, 1070–1073. [PubMed: 11834835]
5. Wong KY (2012). A Retinal Ganglion Cell That Can Signal Irradiance Continuously for 10 Hours. *J. Neurosci.* 32, 11478–11485. [PubMed: 22895730]
6. Dacey DM, Liao H-W, Peterson BB, Robinson FR, Smith VC, Pokorny J, Yau K-W, and Gamlin PD (2005). Melanopsin-expressing ganglion cells in primate retina signal colour and irradiance and project to the LGN. *Nature* 433, 749–754. [PubMed: 15716953]
7. Rea MS, Figueiro MG, Bullough JD, and Bierman A (2005). A model of phototransduction by the human circadian system. *Brain Res. Rev.* 50, 213–228. [PubMed: 16216333]
8. Gooley JJ, Rajaratnam SMW, Brainard GC, Kronauer RE, Czeisler CA, and Lockley SW (2010). Spectral responses of the human circadian system depend on the irradiance and duration of exposure to light. *Sci. Transl. Med* 2, 31ra33.

9. Neitz J, and Neitz M (2011). The genetics of normal and defective color vision. *Vision Res.* 51, 633–651. [PubMed: 21167193]
10. Chen S, and Li W (2012). A color-coding amacrine cell may provide a blue-Off signal in a mammalian retina. *Nat. Neurosci.* 15, 954–956. [PubMed: 22634731]
11. Miyagishima KJ, Grünert U, and Li W (2014). Processing of S-cone signals in the inner plexiform layer of the mammalian retina. *Vis. Neurosci.* 31, 153–163. [PubMed: 24016424]
12. Dacey DM, Peterson BB, and Robinson FR (2002). Identification of an S-cone opponent OFF pathway in the Macaque monkey retina: Morphology, physiology and possible circuitry. *Investig. Ophthalmol. Vis. Sci* 43, eAbstract 2983.
13. Peng YR, Shekhar K, Yan W, Herrmann D, Sappington A, Bryman GS, van Zyl T, Do MTH, Regev A, and Sanes JR (2019). Molecular Classification and Comparative Taxonomics of Foveal and Peripheral Cells in Primate Retina. *Cell* 176, 1222–1237. [PubMed: 30712875]
14. MacNeil MA, and Masland RH (1998). Extreme Diversity among Amacrine Cells: Implications for Function. *Neuron* 20, 971–982. [PubMed: 9620701]
15. Roorda A, and Williams DR (1999). The arrangement of the three cone classes in the living human eye. *Nature* 397, 520–522. [PubMed: 10028967]
16. Liao HW, Ren X, Peterson BB, Marshak DW, Yau KW, Gamlin PD, and Dacey DM (2016). Melanopsin-expressing ganglion cells on macaque and human retinas form two morphologically distinct populations. *J. Comp. Neurol.* 524, 2845–2872. [PubMed: 26972791]
17. Patterson SS, Kuchenbecker JA, Anderson JR, Bordt AS, Marshak DW, Neitz M, and Neitz J (2019). An S-cone circuit for edge detection in the primate retina. *Sci. Rep.* 9, 11913. [PubMed: 31417169]
18. Kolb H, Goede P, Roberts S, Mcdermott R, and Gouras P (1997). Uniqueness of the S-cone pedicle in the human retina and consequences for color processing. *J. Comp. Neurol.* 386, 443–460. [PubMed: 9303428]
19. Mariani AP (1984). Bipolar cells in monkey retina selective for the cones likely to be blue-sensitive. *Nature* 308, 184–186. [PubMed: 6199677]
20. Euler T, Haverkamp S, Schubert T, and Baden T (2014). Retinal bipolar cells: elementary building blocks of vision. *Nat. Rev. Neurosci.* 15, 507–519. [PubMed: 25158357]
21. Dacey DM, and Lee BB (1994). The “blue-on” opponent pathway in primate retina originates from a distinct bistratified ganglion cell type. *Nature* 367, 731–735. [PubMed: 8107868]
22. Calkins DJ, Tsukamoto Y, and Sterling P (1998). Microcircuitry and mosaic of a blue-yellow ganglion cell in the primate retina. *J. Neurosci.* 18, 3373–3385. [PubMed: 9547245]
23. Nasir-Ahmad S, Lee SCS, Martin PR, and Grünert U (2019). Melanopsin-expressing ganglion cells in human retina: Morphology, distribution, and synaptic connections. *J. Comp. Neurol.* 527, 312–327. [PubMed: 28097654]
24. Hannibal J, Tolstrup A, Steffen C, Fahrenkrug J, and Folke J (2017). Melanopsin expressing human retinal ganglion cells: Subtypes, distribution, and intraretinal connectivity. *J. Comp. Neurol.* 525, 1934–1961. [PubMed: 28160289]
25. London M, and Häusser M (2005). Dendritic Computation. *Annu. Rev. Neurosci.* 28, 503–532. [PubMed: 16033324]
26. Koontz MA (1993). GABA-immunoreactive profiles provide synaptic input to the soma, axon hillock, and axon initial segment of ganglion cells in primate retina. *Vision Res.* 33, 2629–2636. [PubMed: 8296458]
27. Koontz MA, Hendrickson AE, and Ryan MK (1989). GABA-immunoreactive synaptic plexus in the nerve fiber layer of primate retina. *Vis. Neurosci.* 2, 19–25. [PubMed: 2487633]
28. Werblin FS (2011). The retinal hypercircuit: A repeating synaptic interactive motif underlying visual function. *J. Physiol.* 589, 3691–3702. [PubMed: 21669978]
29. Sher A, and DeVries SH (2012). A non-canonical pathway for mammalian blue-green color vision. *Nat. Neurosci.* 15, 952–953. [PubMed: 22634728]
30. de Sevilla Muller LP, Shelley J, and Weiler R (2007). Displaced amacrine cells of the mouse retina. *J. Comp. Neurol.* 505, 177–189. [PubMed: 17853452]

31. Kolb H, Linberg KA, and Fisher SK (1992). Neurons of the human retina: A Golgi study. *J. Comp. Neurol.* 318, 147–187. [PubMed: 1374766]
32. Puller C, and Haverkamp S (2011). Bipolar cell pathways for color vision in non-primate dichromats. *Vis. Neurosci.* 28, 51–60. [PubMed: 21070688]
33. Haverkamp S, Wässle H, Duebel J, Kuner T, Augustine GJ, Feng G, and Euler T (2005). The Primordial, Blue-Cone Color System of the Mouse Retina. *J. Neurosci.* 25, 5438–5445. [PubMed: 15930394]
34. Mollon JD (1989). “Tho” she kneel’d in that place where they grew...” The uses and origins of primate colour vision.” *J. Exp. Biol.* 146, 21–38. [PubMed: 2689563]
35. Lucas RJ, Peirson SN, Berson DM, Brown TM, Cooper HM, Czeisler CA, Figueiro MG, Gamlin PD, Lockley SW, O’Hagan JB, et al. (2013). Measuring and using light in the melanopsin age. *Trends Neurosci.* 37, 1–9. [PubMed: 24287308]
36. Spitschan M, Lucas RJ, and Brown TM (2017). Chromatic clocks: Color opponency in non-image-forming visual function. *Neurosci. Biobehav. Rev.* 78, 24–33. [PubMed: 28442402]
37. Moulund JW, Martial F, Watson A, Lucas RJ, and Brown TM (2019). Cones Support Alignment to an Inconsistent World by Suppressing Mouse Circadian Responses to the Blue Colors Associated with Twilight. *Curr. Biol.* 29, 4260–4267. [PubMed: 31846668]
38. Woelders T, Wams EJ, Gordijn MCM, Beersma DGM, and Hut RA (2018). Integration of color and intensity increases time signal stability for the human circadian system when sunlight is obscured by clouds. *Sci. Rep.* 8, 1–10. [PubMed: 29311619]
39. Spitschan M, Aguirre GK, Brainard DH, and Sweeney AM (2016). Variation of outdoor illumination as a function of solar elevation and light pollution. *Sci. Rep.* 6, 1–14. [PubMed: 28442746]
40. Pauers MJ, Kuchenbecker JA, Neitz M, and Neitz J (2012). Changes in the colour of light cue circadian activity. *Anim. Behav.* 83, 1143–1151. [PubMed: 22639465]
41. Packer OS, Verweij J, Li PH, Schnapf JL, and Dacey DM (2010). Blue-Yellow Opponency in Primate S Cone Photoreceptors. *J. Neurosci.* 30, 568–572. [PubMed: 20071519]
42. Field GD, Sher A, Gauthier JL, Greschner M, Shlens J, Litke AM, and Chichilnisky EJ (2007). Spatial properties and functional organization of small bistratified ganglion cells in primate retina. *J. Neurosci.* 27, 13261–13272. [PubMed: 18045920]
43. Grünert U, Jusuf PR, Lee SCS, and Nguyen DT (2011). Bipolar input to melanopsin containing ganglion cells in primate retina. *Vis. Neurosci.* 28, 39–50. [PubMed: 20950505]
44. Della Santina L, Kuo SP, Yoshimatsu T, Okawa H, Suzuki SC, Hoon M, Tsuboyama K, Rieke F, and Wong ROL (2016). Glutamatergic Monopolar Interneurons Provide a Novel Pathway of Excitation in the Mouse Retina. *Curr. Biol.* 26, 2070–2077. [PubMed: 27426514]
45. Anderson JR, Mohammed S, Grimm B, Jones BW, Koshevoy P, Tasdizen T, Whitaker R, and Marc RE (2011). The Viking viewer for connectomics: Scalable multiuser annotation and summarization of large volume data sets. *J. Microsc.* 241, 13–28. [PubMed: 21118201]
46. Cardona A, Saalfeld S, Schindelin J, Arganda-Carreras I, Preibisch S, Longair M, Tomancak P, Hartenstein V, and Douglas RJ (2012). TrakEM2 software for neural circuit reconstruction. *PLoS One* 7, e38011. [PubMed: 22723842]
47. Briggman KL, Helmstaedter M, and Denk W (2011). Wiring specificity in the direction-selectivity circuit of the retina. *Nature* 471, 183–188. [PubMed: 21390125]
48. Bordt AS, Perez D, Tseng L, Liu WS, Neitz J, Patterson SS, Famiglietti EV, and Marshak DW (2019). Synaptic inputs from identified bipolar and amacrine cells to a sparsely branched ganglion cell in rabbit retina. *Vis. Neurosci.* 36, E004. [PubMed: 31199211]
49. Dowling JE, and Boycott BB (1966). Organization of the primate retina: Electron microscopy. *Proc. R. Soc. London. Ser. B* 166, 80–111. [PubMed: 4382694]
50. Tsukamoto Y, and Omi N (2016). ON Bipolar Cells in Macaque Retina: Type-Specific Synaptic Connectivity with Special Reference to OFF Counterparts. *Front. Neuroanat.* 10, 1–20. [PubMed: 26834571]
51. Jusuf PR, Lee SCS, Hannibal J, and Grünert U (2007). Characterization and synaptic connectivity of melanopsin-containing ganglion cells in the primate retina. *Eur. J. Neurosci.* 26, 2906–2921. [PubMed: 18001286]

52. Dacey DM (2004). Origins of perception: Retinal ganglion cell diversity and the creation of parallel visual pathways In *The Cognitive Neurosciences*, Gazzaniga MS, ed. (Cambridge, MA: MIT Press), pp. 281–301.
53. Dhande OS, Stafford BK, Franke K, El-Danaf R, Percival KA, Phan AH, Li XP, Hansen BJ, Nguyen PL, Berens P, et al. (2019). Molecular Fingerprinting of On-Off Direction-Selective Retinal Ganglion Cells Across Species and Relevance to Primate Visual Circuits. *J. Neurosci.* 39, 78–95. [PubMed: 30377226]
54. Tsukamoto Y, and Omi N (2015). OFF bipolar cells in macaque retina: type-specific connectivity in the outer and inner synaptic layers. *Front. Neuroanat.* 9, 1–17. [PubMed: 25657619]
55. Puthussery T, Gayet-Primo J, Taylor WR, and Haverkamp S (2011). Immunohistochemical identification and synaptic inputs to the diffuse bipolar cell type DB1 in macaque retina. *J. Comp. Neurol.* 519, 3640–3656. [PubMed: 22006647]
56. Chun M-H, Moon J-I, Jeon JH, Kim I-B, Kim H-L, Koo T-H, Lee U-Y, Jeong E, and Massey SC (2012). Axonal Synapses Utilize Multiple Synaptic Ribbons in the Mammalian Retina. *PLoS One* 7, e52295. [PubMed: 23284975]
57. Østergaard J, Hannibal J, and Fahrenkrug J (2007). Synaptic contact between melanopsin-containing retinal ganglion cells and rod bipolar cells. *Investig. Ophthalmol. Vis. Sci.* 48, 3812–3820. [PubMed: 17652756]

Patterson *et al.* identify a new amacrine cell type in the primate retina with “blue” S-cone circuit input and targeted output to intrinsically photosensitive retinal ganglion cells (ipRGCs). This circuit may contribute to the effects of short-wavelength light on ipRGC downstream non-image-forming visual functions like sleep, mood and learning.

- 3D reconstruction of the S-cone connectome revealed S-cone selective amacrine cells
- S-cone amacrine cells receive excitatory input from only S-cone ON bipolar cells
- S-cone amacrine cells make targeted inhibitory synapses onto ipRGCs
- Resulting short-wavelength sensitivity is distinct from that mediated by melanopsin

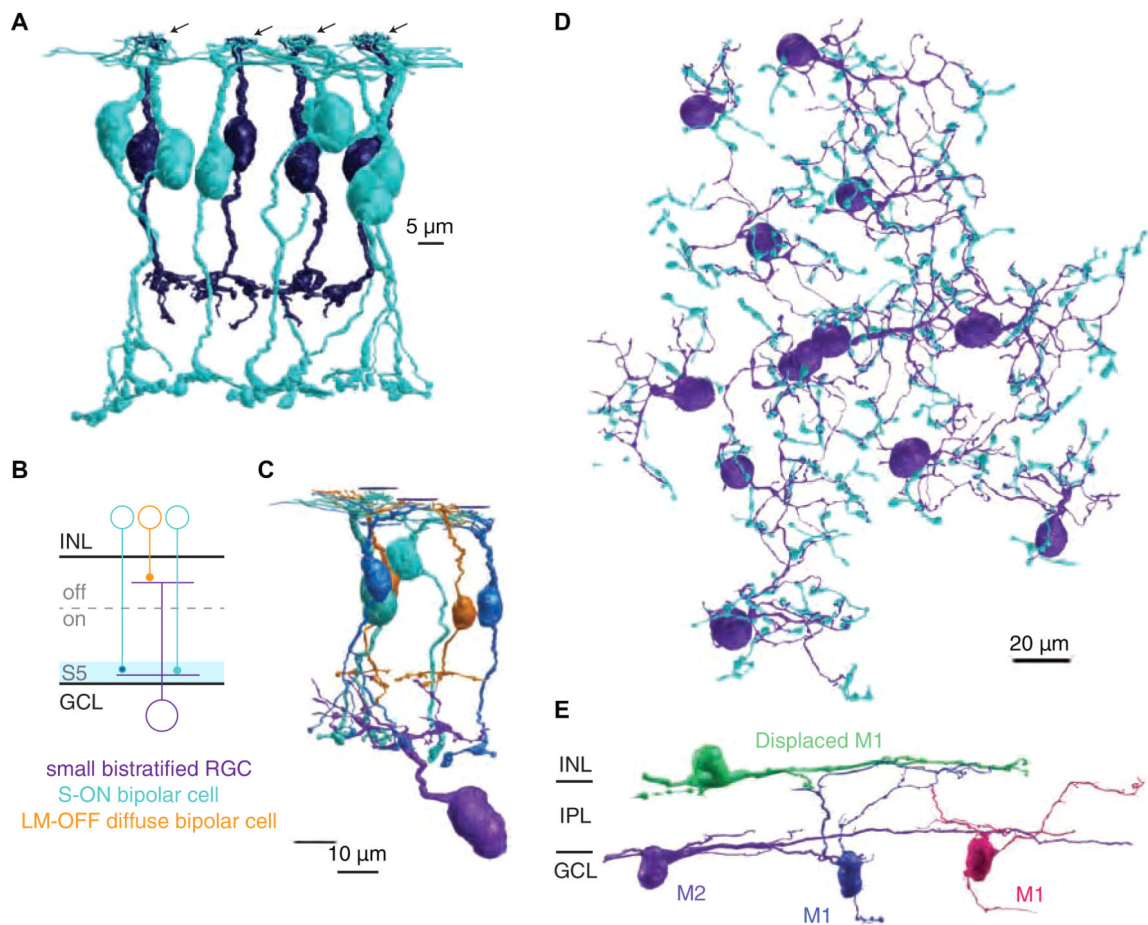


Figure 1. Serial EM reconstruction of ipRGCs and the S-cone connectome in primate retina. (A) Four representative S-cones (arrows) and their S-ON bipolar cell (blue) and OFF midwidge bipolar cell (purple) contacts. (B) Small bistratified RGC circuit used for verification of S-cone and S-ON bipolar cell identification. (C) 3D reconstruction of the small bistratified RGC circuit in 1B. (D) 60 S-ON bipolar cell terminals contacting 12 small bistratified RGCs. (E) 3D reconstructions of the major ipRGC subtypes in primate retina. Note the ipRGC dendrites are monostratified but appear curved as the volume slopes away from the fovea.

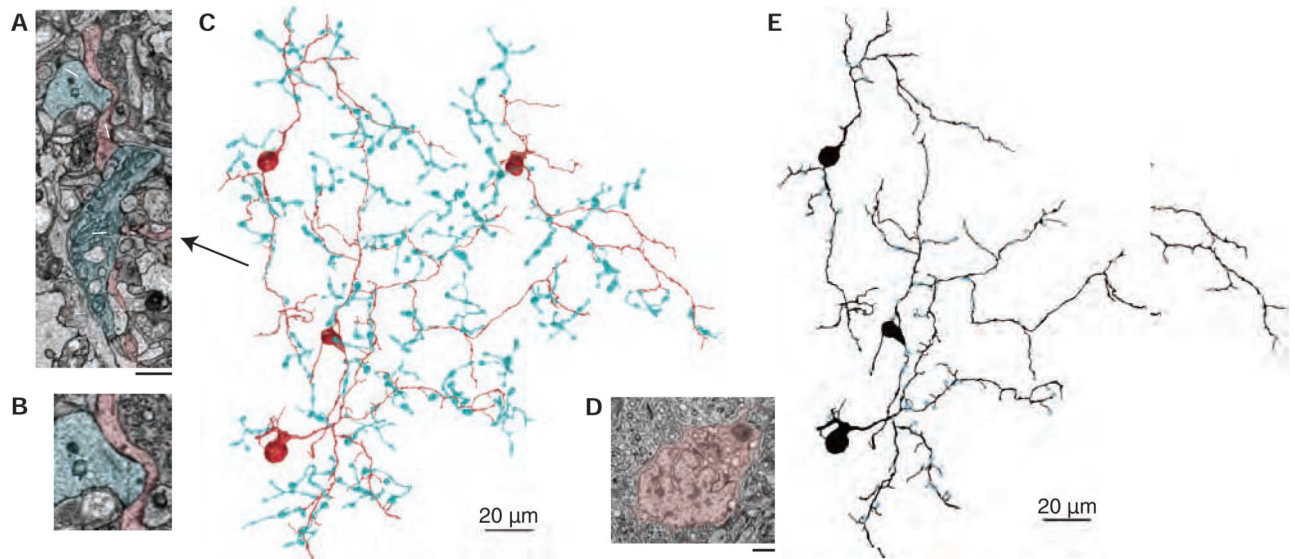


Figure 2. Identification of an S-cone exclusive amacrine cell.

(A) Electron micrographs of three ribbon synapses (white arrows) from an S-ON bipolar cell (cyan) to an S-cone amacrine cell (red). Scale bar is 1.5 μm . (B) Inset from 2A showing two S-ON bipolar cell ribbon synapses. (C) 3D reconstructions of S-ON bipolar cell axon terminals providing input to four S-cone amacrine cells (red). (D) S-cone amacrine cells are easily identifiable by their asymmetric nuclei offset from the center of their soma. Scale bar is 1 μm . (E) Locations of S-ON bipolar cell input (blue) to three S-cone amacrine cells.

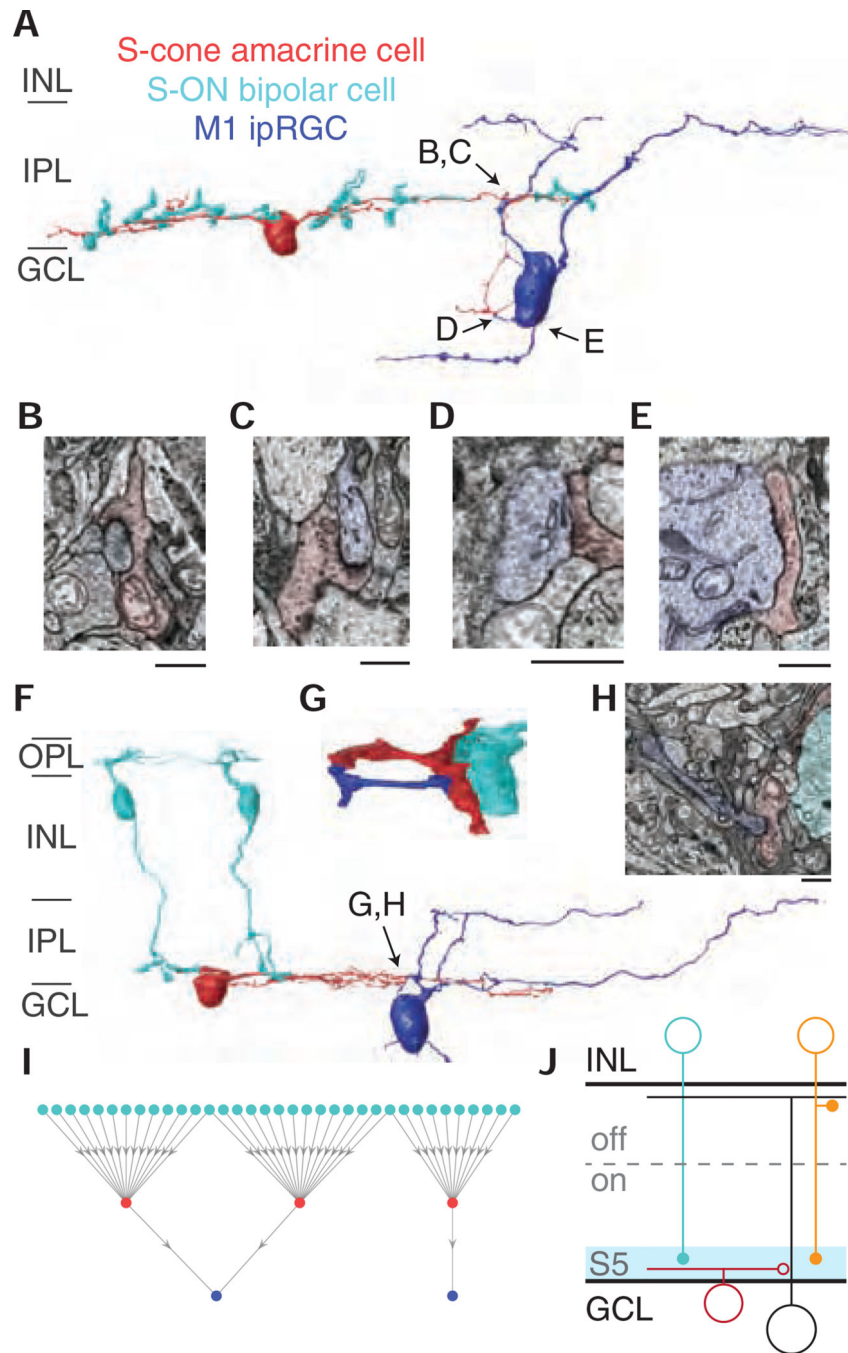


Figure 3. M1 ipRGCs receive targeted inhibitory input from S-cone amacrine cells. (A) 3D reconstruction of an M1 ipRGC receiving synaptic input from an S-cone amacrine cell. The S-cone amacrine cell dendrite travels into the ganglion cell layer to provide additional synaptic input to the M1 ipRGC soma. See also Video S1. (B-E) Four electron micrographs of the synapses in 3A. (F) 3D reconstruction of S-cone amacrine cell input to an M1 ipRGC, with complete reconstructions of two representative S-ON bipolar cells. (G) Detailed reconstruction of S-cone amacrine cell to ipRGC synaptic contact. (H) Synapse from an S-cone amacrine cell to the M1 ipRGC in 3F and 3H. Scale bar is 1 μ m. (I)

Network of S-ON bipolar cells, S-cone amacrine cells and M1 ipRGCs. **(J)** Circuit diagram of cone-opponent inputs to ipRGCs. *En passant* synapses from ON diffuse bipolar cells (orange) contribute to the LM-ON response [16,43].

Author Manuscript

Author Manuscript

Author Manuscript

Author Manuscript